Available online at www.sciencedirect.com
ScienceDirect
Journal of the European Ceramic Society 28 (2008) 1037–1042
www.elsevier.com/locate/jeurceramsoc

SiOC ceramic with high excess free carbon

Hans-Joachim Kleebe [a,*], Yigal D. Blum [b]

[a] Technische Universität Darmstadt, Institute of Applied Geosciences, Geomaterial Science, D-64287 Darmstadt, Germany
[b] Chemical Science and Technology Laboratory, SRI International, Menlo Park, CA 94025, USA

Abstract

The correlation between microstructure evolution and increasing processing temperature of a polymer-derived SiOC ceramic with a high volume fraction of free carbon was studied by transmission electron microscopy (TEM). The high carbon content of the SiOC ceramic was achieved by crosslinking the starting precursor polyhydridomethylsiloxane (PHMS) with divinylbenzene (DVB). Focus of the TEM characterization was the evolution of the carbon phase upon pyrolysis at 1000 °C and after additional heat treatment at 1450 °C. Although a continuous structural rearrangement within the bulk SiOC matrix was observed with raising temperature, the sample annealed at 1450 °C remained predominantly amorphous, with the exception of a percolation network of turbostratic carbon and a slight precipitation of nanosized SiC particles. The micro/nanostructure observed in this sample upon thermal treatment at high-temperature suggests a phase separation in small SiO_4- and SiC_4-rich regions encapsulated by carbon. This specific phase distribution is consistent with the exceptional thermo-mechanical properties reported for similar high C-content SiOC materials.

Keywords: Polymer-derived ceramics; SiOC; Carbon content; Microstructure; Transmission electron microscopy

1. Introduction

Compared to fused SiO_2, carbon-rich SiOC glasses reveal superior mechanical properties at elevated temperatures, in particular, improved creep and oxidation resistance.[1–3] Saha et al. reported on the viscoelastic response of SiOC(C) at 1300 °C, when an external load was successively applied and released, and the authors developed a model of the corresponding nanostructure, which will be discussed in this paper.

The incorporation of a high carbon content into the fused silica glass structure is extremely difficult, if not impossible, when for example mixing carbon black or graphite with molten silica.[4] Therefore, most SiOC glasses reported in literatures, containing excess free carbon, were synthesized by the sol–gel route. This processing routine enables the formation of a homogeneous glass network (at the molecular level) at a rather low pyrolysis temperature.[5–8] In addition, this approach offers the ability to easily tailor various compositions by mixing corresponding starting alkoxides in different molar ratios,[7] where a T^H/D^H ratio of 2 theoretically yields a stoichiometric SiOC glass without the residual free carbon phase. T^H represents $HSiO_3$ units, derived from $HSi(OR)_3$, while D^H stands for CH_3SiHO_2 units, prepared from a $CH_3SiH(OR)_2$ precursor. In comparison, the starting precursor polyhydridomethylsiloxane (PHMS), used for processing the carbon-rich SiOC material studied here, is predominantly made of D^H units, which either convert to pseudo D^H units when reacted with alkenes, or to T^H units when reacting with water.[9]

In general, such a SiOC network can be generated by the substitution of two divalent oxygen ions by one tetravalent carbon ion within the SiO_2 network. The composition of a stoichiometric SiOC, consisting solely of Si–O and Si–C bonds, is given by $SiC_xO_{2(1-x)}$. Since excess free carbon is incorporated into the SiOC glass network, $C(Si)_4$ units are locally formed, which results in a strengthened glass network, owing the locally increased bond strength, which also explains the improved resistance against creep deformation as well as the reported rise in glass-transition temperature, T_g, viscosity, η, Young's modulus, E and hardness, H, all of which increase with an increased incorporation of carbon into the glass network structure.[10,11]

Heat-treatment at 1000 °C commonly yields amorphous SiOC solids, which contain a small molar ratio of residual hydrogen as well as residual free carbon; the latter being the focus of this paper.[3,12] Annealing temperatures exceeding 1100 °C promote local decomposition within the matrix due to the escape of gaseous species such as SiO, CO and/or CH_4.

* Corresponding author. Tel.: +1 49 6151 164554; fax: +1 49 6151 164021.
E-mail address: keebe@geo.tu-darmstadt.de (H.-J. Kleebe).

0955-2219/$ – see front matter © 2007 Published by Elsevier Ltd.
doi:10.1016/j.jeurceramsoc.2007.09.024

The decomposition process is accompanied by the formation of nanosized SiC crystallites embedded in the amorphous matrix, as confirmed by transmission electron microscopy (TEM).[13–20]

In a previous TEM/EELS study it was shown that a stoichiometric SiOC sample revealed a phase separation process, $SiC_xO_{2(1-x)} \Rightarrow xSiC + (1-x)SiO_2$, which started at ~1200 °C and resulted in the formation of nanosized SiC precipitates finely dispersed in the amorphous SiO_2-rich bulk.[13] The phase separation into crystalline SiC and amorphous SiO_2 was shown to progress with increasing temperature. A variety of polymer-derived ceramics (PDC's) were characterized by high-resolution TEM [20] and it was reported that the first nucleation event typically observed was the formation of excess free carbon, followed by the nucleation of SiC. It was concluded that the presence of SiC nanocrystals was associated with the progression of local carbothermal reduction, $SiO_2 + 3C \Rightarrow SiC + 2CO_{(g)}$. Two non-stoichiometric SiOC materials ($T^H/D^H = 1$ and 9) were characterized by TEM in conjunction with electron energy-loss spectroscopy (EELS). The study showed that the SiOC glasses were either enriched in carbon or silicon.[21] The Si-rich SiOC matrix revealed pronounced grain growth of the Si precipitates upon annealing at 1300 °C for 100 h. The observed grain coarsening is consistent with the classical Ostwald ripening model of spherical particles embedded in an amorphous matrix.[22] The analysis of the size variation with time allowed the determination of a diffusion coefficient of Si in SiOC of 10^{-16} cm^2/s, which is consistent with Si volume diffusion in amorphous SiO_2. In general, TEM studies confirmed the metastable nature of such polymer-derived SiOC glasses, since crystallization into thermodynamically stable phases occurred upon subsequent thermal treatment. It is interesting to note though that the formation of crystalline SiO_2 phases such as crystobalite or tridymite is not observed in these materials.

The one SiOC material characterized here, PHMS + 60%DVB, contains a much higher carbon content as compared to similar SiOC samples prepared via the sol–gel route. The microstructure evolution, in particular the evolution of the carbon phase, was studied with emphasis on the correlation between micro/nanostructure and the corresponding thermo-mechanical response.

2. Experimental procedures

Preceramic polymers were synthesized by modifying and curing polyhydrido-methylsiloxane (PHMS).[23] The high carbon content was tailored by mixing PHMS with 60 wt.% divinylbenzene (DVB). The DVB was first mixed with a diluted solution of a platinum-divinyltetramethyldisiloxane-catalyst in xylene (5 ppm relative to PHMS) and then added to the low viscosity PHMS. The blend was stirred for about 20 min in dry environment, cast in a dish to form 2–3 mm thick specimens and cured at room temperature for 12 h. A brittle rubbery solid is obtained. Additional curing was carried out at 120 °C overnight in air. Both reactions were performed in a liquid phase with no solvents added (except for diluting the Pt catalyst), leading to a dense, cured polymeric, resin-like SiOC material. Subsequently, the cured preceramic bulk specimen was pyrolyzed under flowing Ar-atmosphere in a Lindberg tube furnace, equipped with a sealed alumina tube and inert gas flow system, using a heating rate of 5 °C/min and a holding time of 1 h at 1000 °C (pyrolysis) and 1450 °C (annealing). Elemental analyses of the pyrolysed sample was performed by Galbraith Laboratories, USA, and revealed an overall composition of $SiC_{0.44}O_{1.13}$ + 2.27% C_{free} which relates to 37.7 vol.% of excess free carbon.

Transmission electron microscopy (TEM) imaging and electron diffraction pattern (EDP) analysis were performed on TEM-foils obtained from the bulk pyrolysed and annealed SiOC samples. Sample preparation followed the standard ceramographic technique of cutting, ultrasonic drilling, dimpling and Ar-ion thinning to perforation followed by light carbon coating to minimize charging under the incident electron beam. The instrument used was a Philips CM20STEM (FEI, Eindhoven, The Netherlands) operating at 200 keV.

3. Results

The data presented focus on a detailed micro/nanostructure characterization of one polymer-derived SiOC material. In particular, the question of the influence of excess free carbon, a common impurity in those materials which results from the organic precursors employed as starting materials, on the high-temperature stability and thermo-mechanical response of the amorphous network is addressed.

Since the SiOC material was not processed by dissolving elemental carbon into molten silica, a processing route which was shown to be rather unsuccessful[4], but by well-controlled pyrolysis of crosslinked PHMS, $[CH_3SiHO]_n$, a unique molecular arrangement of the intrinsic polymer architecture was achieved.

Transmission electron microscopy (TEM) allows the imaging of local structures that formed upon pyrolysis or after subsequent thermal treatment.[24–26] The pyrolysis temperature of the PHMS + 60%DVB specimen was 1000 °C, while the high-temperature anneal was performed at 1450 °C for 1 h. As often reported for polymer-derived ceramics (PDCs) after pyrolysis [27–29], this SiOC sample also exhibited a completely amorphous microstructure. A random glass network was observed by high-resolution TEM (HRTEM) imaging, as depicted in Fig. 1(a).

Electron diffraction analysis of the pyrolysed and annealed sample confirmed the trend observed by HRTEM imaging (Fig. 1(a) and (b)): a considerable rearrangement of the glass network, leading to the formation of a high volume fraction of turbostratic carbon in the otherwise predominantly amorphous SiO_2/SiC matrix. It is interesting to note that heat-treatment of amorphous SiOC at temperatures exceeding the pyrolysis temperature results in the formation of turbostratic carbon, and SiC nanocrystals as will be shown later, whereas the formation of crystalline SiO_2 phases such as tridymite or cristobalite was not detected.

The radial intensity profile of the corresponding electron diffraction pattern (EDP) of the pyrolysed PHMS + 60%DVB sample revealed only a weak intensity at ~4.8 nm^{-1}, which can be assigned to the spacing of carbon atoms in isolated graphene layers (0.21 nm).[30] However, the corresponding HRTEM image did not reveal any nanostructural feature that could be corre-

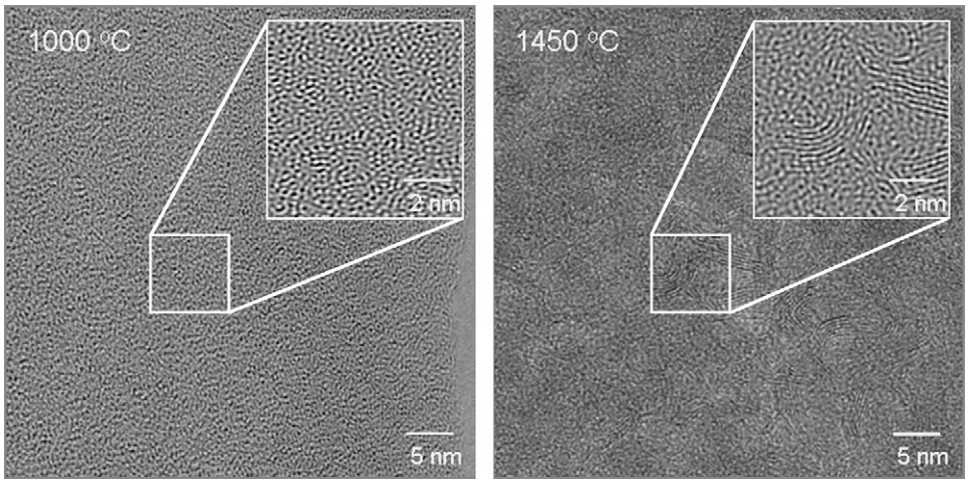

Fig. 1. (a) HRTEM image of the amorphous structure of the PHMS + 60%DVB sample upon pyrolysis at 1000 °C. The inset shows an enlarged Fourier-filtered image of the boxed region. (b) HRTEM image of the sample shown in (a); however, after subsequent annealing at 1450 °C. Note the pronounced formation of a turbostratic carbon phase, which is not visible in (a).

lated with the presence of this carbon phase. The absence of an EDP signal at 0.33 nm, the (0 0 0 2) lattice spacing of graphite, indicates that the graphene layers are not yet well-stacked rather than being finely dispersed throughout the amorphous matrix and hence could not be detected by HRTEM imaging (Fig. 1(a)).

The radial intensity profile of the annealed sample showed that the heat-treatment at 1450 °C induces a pronounced structural rearrangement, which is consistent with ^{13}C NMR data reported on this material.[23] Note that the ^{13}C NMR study confirmed a distinct separation in sp^2 and sp^3 carbon environments, with a high fraction of aromatic carbon already at 800 °C, which is seen as evidence for the presence of isolated graphene layers at low pyrolysis temperature. The corresponding EDP intensities can be assigned to a SiC environment at 3.9, 7.0 and 7.5 nm^{-1} and to a graphite environment at 3.0, 4.8 and 8.3 nm^{-1}. Hence, high-temperature anneal results in the formation of turbostratic carbon, where the graphene layers are now well-stacked ontop of each other, given a spacing between the graphene layers along the *c*-axis of 0.33 nm.

Scarmi et al. reported on a very interesting and unexpected observation: the viscoelastic behaviour of carbon-rich SiOC at temperatures exceeding 1000 °C.[31] In brief, their experiment was performed as follows: when loading pure SiO_2 glass in compression at 1000 °C, an expected high-temperature creep deformation was monitored. However, when continuously loading and unloading the SiOC sample at a slightly higher temperature, the initial strain was recovered after the applied stress was removed from the sample. Scrami et al. proposed two different SiOC nanostructure models regarding the distribution of the carbon phase within the residual amorphous silica. In the first model, the carbon phase was embedded in a SiO_2 matrix as isolated individual clusters, while the second model predicted graphene cages, which encapsulated the SiO_2 glass phase. A schematic illustration of the two models is given in Fig. 2.

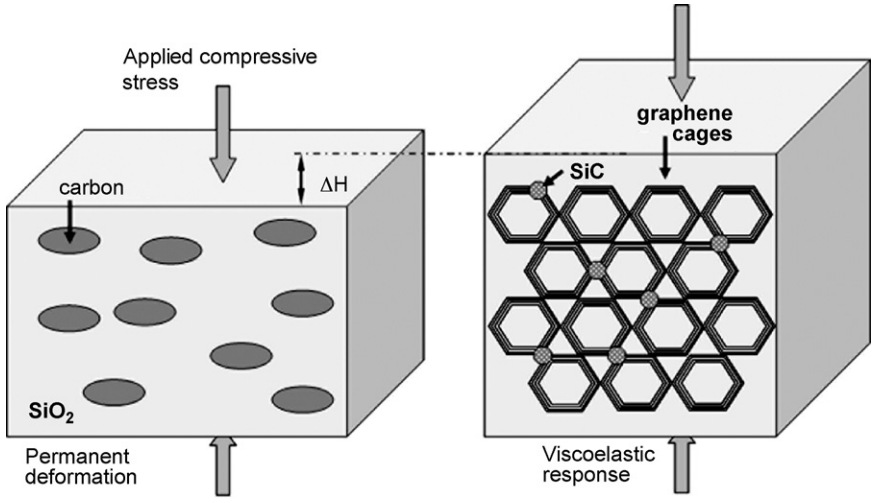

Fig. 2. Schematic showing the two potential models of the carbon dispersion within the SiOC bulk proposed in Ref. 31. (a) Isolated carbon clusters embedded in the remaining SiO_2 phase and (b) graphene cages encapsulating the amorphous silica. Note that only the model depicted in (b) can explain the viscoelastic behaviour of SiOC with a high fraction of excess free carbon.

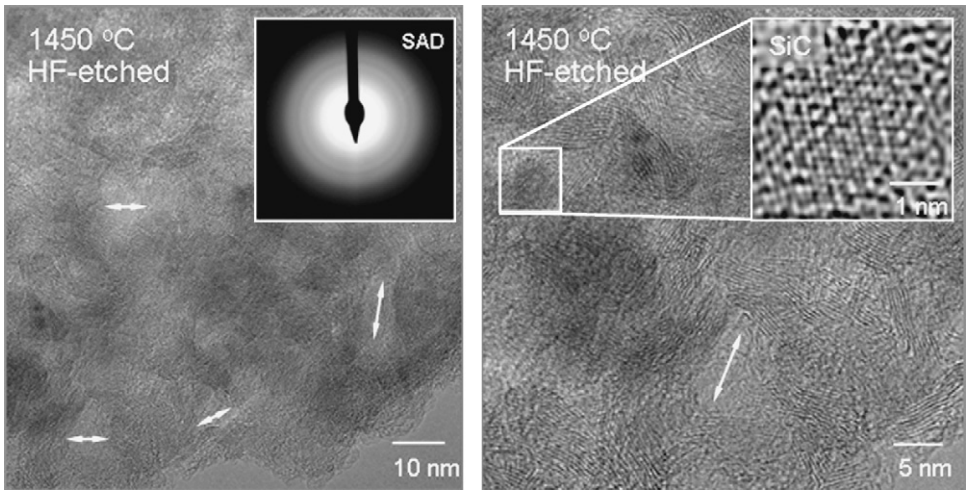

Fig. 3. (a) HRTEM image of the thermally treated PHMS + 60%DVB sample after HF-etching. It is assumed that the etching process selectively removed the residual silica phase forming small pores (indicated by arrows) with an average diameter of 10–20 nm. (b) HRTEM image of the same sample shown in (a). The enlarged area clearly shows the formation of nanosized SiC crystallites in close proximity to the turbostratic carbon (graphene cages).

Only the second model could explain the observed viscoelastic behaviour of the carbon-rich SiOC. When applying a compressive stress, the graphene cages will be deformed together with the entrapped SiO_2 glass phase. In contrary, when releasing the applied compressive stress, the graphene cages can gradually return to their original shape dragging the encaged silica phase along, resulting in no permanent creep deformation.

In order to verify as to whether such a nanostructure model (Fig. 2(b)) indeed represents the intrinsic microstructure of the annealed carbon-rich PHMS + 60%DVB sample studied here, HF-etching was performed on a dimpled TEM foil, in order to selectively remove the residual SiO_2 phase. The resulting microstructure is shown in the HRTEM image of Fig. 3(a).

As shown in Fig. 3, the nanostructure of the annealed, HF-etched sample revealed small pores close to the edge of the TEM foil. It is concluded that the residual silica phase was selectively etched creating the observed residual porosity with pore diameters of 10–20 nm. SiC nanocrystals were detected in the PHMS + 60%DVB sample in close proximity to the turbostratic carbon. The fraction of carbon atoms that are directly bonded to silicon is rather high in the DVB-containing sample, as compared to a stoichiometric SiOC material. Therefore, a higher fraction of thermodynamically stable SiC crystallites was expected to form at elevated temperature.

4. Discussion

Turbostratic carbon can easily be detected within an amorphous bulk by HRTEM; however, only when the (0 0 0 2) graphite lattice planes are oriented perpendicular to the image plane, i.e., parallel to the incident electron beam. The number of layers constituting the turbostratic structure has probably to be higher than three or four to allow an unequivocal distinction of turbostratic carbon by HRTEM. Consequently, due to electron optical limitations, regions with excess free carbon composed only of one or two graphene layers are commonly not distinguishable from the surrounding amorphous SiOC network by HRTEM. Therefore, it is deduced that the nanostructure of the pyrolyzed PHMS + 60%DVB sample contains a large number of well-dispersed graphene sheets (aromatic carbon), being consistent with a previous ^{13}C NMR analysis,[23] which however cannot be recorded by HRTEM (cf. Fig. 1(a)). Upon exposure to 1450 °C, the SiOC glass network undergoes a marked reconfiguration by rearranging the excess free carbon phase. At elevated temperature, the initially finely dispersed graphene layers grow and form multi-layered turbostratic carbon, as shown in Fig. 3.

While nucleation within the binary Si–C system was reported to start at temperatures as low as 900 °C, crystallization within the ternary Si–C–N and Si–O–C systems was observed at temperatures exceeding 1100 °C.[20,32] In contrast, the quaternary Si–C–N–O system remained amorphous at temperatures even exceeding 1400 °C. A number of studies focused on the properties and microstructure evolution of Si–B–C–N ceramics and monitored a higher thermal stability of this quaternary system.[33–35] Using HRTEM imaging it was observed that thin turbostratic B(C)N layers had formed in close proximity to Si_3N_4-rich regions. It was concluded that such layers, forming a kind of percolation network in the otherwise amorphous matrix, act as diffusion barriers that prevent local crystallization by keeping the size of the nucleus below the critical radius, R_c. Note that a similar percolation network of the turbostratic carbon was observed in the annealed PHMS + 60%DVB sample.

An interesting question to address is where in carbon-rich SiOC materials the Si–C bonds and thus the SiC_4 units are located. Upon exposure to 1450 °C, carbon atoms can only bond to either other carbon atoms or directly to silicon. Within the graphene layers, carbon atoms are all bonded to each other and do not reveal out-of-planes bonds. The graphene sheets are chemically stable and hence do not react with the exception of carbon atoms at their molecular edges. Therefore, it is assumed that most of the edges of the graphene layers are bonded to either Si or to oxygen forming mixed SiO_xC_y units. However, it is expected that, in particular at higher temperatures, the formation of mixed units is thermodynamically not

favorable. The observed fraction of SiC crystallites (Fig. 3(b)) can also be a result from a local carbothermal reduction of silica, $SiO_2 + 3C \rightarrow SiC + 2CO$, which is commonly monitored at temperatures exceeding 1300 °C. However, the rather low weight loss of approximately 6% determined after exposure to 1500 °C for 1 h suggests that carbothermal reduction is not a dominating process in this sample, despite its high carbon content.

Therefore, it can be concluded that carbothermal reduction occurs only at the edges of the graphene layers forming SiC nanocrystals in close proximity to the turbostratic carbon, resulting in the nanostructure depicted in Fig. 3(b). Since HF-etching generated small pores in the order of 10–20 nm in diameter, as indicated by arrows, the SiO_2-rich regions must be of a similar dimension. However, it cannot be excluded that a small fraction of mixed SiO_xC_y units were also etched by hydrofluoric acid. The overall micro/nanostructure observed in the annealed PHMS + 60%DVB sample closely reflects the second structural model shown in Fig. 2(b), which is consistent with the thermomechanical behaviour of a similar carbon-rich SiOC material, i.e., with the viscoelastic behaviour at elevated temperature.

However, there is still an open question regarding the transport mechanism of the carbon phase through the amorphous matrix. Although the intrinsic density of such SiOC glasses is rather low, it is counterintuitive that entire graphene sheets migrate though the glass network. In contrast, it is thought that the overall micro/nanostructure evolution of this sample is closely related to the intrinsic architecture of the starting precursor employed for synthesis. A recent study by Störmer et al. conclusively showed that depending on the architecture of the starting SiCN polymer, different nanostructures and thermal stabilities result upon thermal annealing. Hence it was concluded that some of the glass structures "memorize" the polymer architecture, which in turn affects the nanostructure evolution at high-temperature. In contrast, it is well-established from NMR data that major molecular rearrangements in SiCN and SiOC systems occur,[36] so that for the material discussed here, the incorporation and dispersion of the high excess free carbon content may not be governed by the initial architecture of the starting polymer. The observed microstructural variations, in particular of the carbon phase, support the latter view.

5. Conclusions

One carbon-rich, polymer-derived SiOC ceramic was studied by transmission electron microscopy to follow the nanostructure evolution, in particular of the excess free carbon phase, upon pyrolysis and subsequent thermal treatment at 1450 °C. High-resolution TEM did not allow imaging of the excess free carbon phase, which however could already be detected by ^{13}C NMR even below the pyrolysis temperature. Upon additional heat-treatment, the carbon phase undergoes severe rearrangement leading to the formation of a percolation network of turbostratic carbon by growth and ordered stacking of graphene layers. Carbothermal reduction is strongly suppressed in this material resulting in the formation of SiC nanocrystals only in close proximity to the turbostratic carbon. The overall nanostructure formed in this sample at high-temperature is characterized by small SiO_2-rich regions engulfed by turbostratic carbon which again is connected by SiC nanocrystals. This particular phase arrangement is responsible for a viscoelastic response at high-temperature. Moreover, it is thought that the nanostructural evolution observed is not a consequence of the specific polymer architecture employed during processing, but a result of pronounced molecular rearrangements upon thermal anneal.

Acknowledgement

This work was partly supported by the Ceramics Program of the National Science Foundation (NSF) under the contract No. DMR-0304968.

References

1. Renlund, G. M., Prochazka, S. and Doremus, R. H., Silicon oxycarbide glasses. Part I: Preparation and chemistry and Part II: Structure and properties. *J. Mater. Res.*, 1991, **6**, 2716–2734.
2. Sorarù, G. D., Dallapiccola, E. and D'Andrea, G., Mechanical characterization of sol–gel-derived silicon oxycarbide glasses. *J. Am. Ceram. Soc.*, 1996, **79**, 2074–2080.
3. Pantano, C. G., Singh, A. K. and Zhang, H., Silicon carbide glasses. *J. Sol–Gel Sci. Technol.*, 1999, **14**, 7–25.
4. Elmer, T. H. and Meissner, H. E., Increase of annealing point of 96% SiO_2-glass on incorporation of carbon. *J. Am. Ceram. Soc.*, 1976, **59**, 206–209.
5. Zhang, H. and Pantano, C. G., Synthesis and characterization of silicon oxycarbide glasses. *J. Am. Ceram. Soc.*, 1990, **73**, 958–963.
6. Hammond, M., Breval, E. and Pantano, C. G., Microstructure and viscosity of hot pressed silicon oxycarbide glasses. *Ceram. Eng. Sci. Proc.*, 1993, **14**, 947–954.
7. Sorarù, G. D., Andrea, G. D. and Campostrini, R., Structural characterization and high-temperature behavior of silicon oxycarbide glasses prepared from sol–gel precursors containing Si–H bonds. *J. Am. Ceram. Soc.*, 1995, **78**, 379–387.
8. Blum, Y. D. and MacQueen, D. B., Modification of hydrosiloxane polymers for coating applications. *Surf. Coat. Int. Part B1*, 2001, **84**, 27–33.
9. Blum, Y. D., MacQueen, D. B. and Kleebe, H.-J., Synthesis and characterization of carbon enriched silicon oxycarbides. *J. Eur. Ceram. Soc.*, 2005, **25**, 143–149.
10. Rouxel, T., Massouras, G. and Sorarù, G. D., High-temperature behavior of an SiOC oxycarbide glass: elasticity and viscosity. *J. Sol–Gel Sci. Technol.*, 1999, **14**, 83–94.
11. Bodet, R., Jia, N. and Tressler, R. E., Microstructural instability and the resultant strength of Si–C–O (Nicalon) and Si–N–C–O (HPZ) fibres. *J. Eur. Ceram. Soc.*, 1996, **16**, 653–657.
12. Breval, E., Hammond, M. and Pantano, C. G., Nanostructural characterization of silicon oxycarbide glasses and glass-ceramics. *J. Am. Ceram. Soc.*, 1994, **77**, 3012–3018.
13. Kleebe, H.-J., Turquat, C. and Sorarù, G. D., Phase separation in a SiCO glass studied by transmission electron microscopy and electron energy-loss spectroscopy. *J. Am. Ceram. Soc.*, 2001, **84**, 1073–1080.
14. Kleebe, H.-J., Suttor, D., Müller, H. and Ziegler, G., Decomposition-crystallization of polymer-derived Si–C–N ceramics. *J. Am. Ceram. Soc.*, 1998, **81**, 2971–2977.
15. Kleebe, H.-J., Störmer, H., Trassl, S. and Ziegler, G., Thermal stability of SiCN ceramics studied by spectroscopy and electron microscopy. *Appl. Organomet. Chem.*, 2001, **15**, 858–866.
16. Traßl, S., Suttor, D., Motz, G., Rössler, E. and Ziegler, G., Structural characterisation of silicon carbonitride ceramics derived from polymeric precursors. *J. Eur. Ceram. Soc.*, 2000, **20**, 215–225.
17. Traßl, S., Motz, G., Rössler, E. and Ziegler, G., Characterization of the free-carbon phase in precursor-derived Si–C–N ceramics. I. Spectroscopic methods. *J. Am. Ceram. Soc.*, 2002, **85**, 239–244.

18. Traßl, S., Kleebe, H.-J., Störmer, D., Motz, G., Rössler, E. and Ziegler, G., Characterization of the free-carbon phase in precursor-derived Si–C–N ceramics. II. Comparison of different polysilazane precursors. *J. Am. Ceram. Soc.*, 2002, **85**, 1268–1274.
19. Gregori, G., Kleebe, H.-J., Brequel, H., Enzo, S. and Ziegler, G., Microstructure evolution of precursors-derived SiCN ceramics upon thermal treatment at temperatures ranging between 1000 and 1400 °C. *J. Non-Cryst. Solids*, 2005, **351**, 1393–1402.
20. Monthioux, M. and Delverdier, O., Thermal behavior of (organosilicon) polymer-derived ceramics. V. Main facts and trends. *J. Eur. Ceram. Soc.*, 1996, **16**, 721–737.
21. Turquat, C., Kleebe, H.-J., Gregori, G., Walter, S. and Sorarù, G. D., TEM and EELS study of non-stoichiometric SiCO glasses. *J. Am. Ceram. Soc.*, 2001, **84**, 2189–2196.
22. Gregori, G., Kleebe, H.-J. and Sorarù, G. D., Energy-filtered TEM study of ostwald ripening of Si nanocrystals in SiCO glasses. *J. Am. Ceram. Soc.*, 2006, **89**, 1699–1703.
23. Kleebe, H.-J., Gregori, G., Babonneau, F., Blum, Y. D., MacQueen, D. B. and Masse, S., Evolution of C-rich SiOC ceramics. Part-I: characterization by integral spectroscopic techniques: solid-state NMR and Raman spectroscopy. *Int. J. Mater. Res.*, 2006, **97**, 699–709.
24. Riedel, R., Kleebe, H.-J., Schönfelder, H. and Aldinger, F., A covalent micro/nano-composite resistant to high-temperature oxidation. *Nature*, 1995, **374**, 526–528.
25. Zern, A., Mayer, J., Narayanan, J., Weinmann, M., Bill, J. and Rühle, M., Quantitative EFTEM-study of precursor-derived ceramics. *J. Eur. Ceram. Soc.*, 2002, **22**, 1621–1627.
26. Kaneko, K. and Kakimoto, K.-I., HRTEM and ELNES analysis of polycarbosilane-derived Si-C-O bulk ceramics. *J. Non-Cryst. Solids*, 2000, **270**, 181–190.
27. Gregori, G., Kleebe, H.-J., Blum, Y. D. and Babonneau, F., Evolution of C-rich SiOC ceramics. Part-II: Characterization by high lateral resolution techniques: electron energy-loss spectroscopy, high-resolution tem and energy-filtered TEM. *Int. J. Mater. Res.*, 2006, **97**, 710–720.
28. Pederiva, L., Sorarù, G. D., LaTournerie, J. and Raj, R., Pyrolysis kinetics for the conversion of a polymer into an amorphous ceramic. *J. Am. Ceram. Soc.*, 2002, **85**, 2181–2187.
29. Störmer, H., Kleebe, H.-J. and Ziegler, G., Metastable SiCN glass matrices studied by energy-filtered electron diffraction pattern analysis. *J. Non-Cryst. Solids*, 2007, **353**, 2867–2877.
30. Amelinckx, S., Lucas, A. and Lambin, P., Electron diffraction and microscopy of nanotubes. *Rep. Prog. Phys.*, 1999, **62**, 1471–1524.
31. Scarmi, A., Sorarù, G. D. and Raj, R., The Role of carbon in unexpected visco(an)elastic behavior of amorphous silicon oxycarbide above 1273 K. *J. Non-Cryst. Solids*, 2005, **351**, 2238–2243.
32. Amkreutz, M. and Frauenheim, T., Understanding precursor-derived amorphous Si–C–N ceramics on the atomic scale. *Phys. Rev. B*, 2002, **65**, 134113.
33. Bill, J. and Aldinger, F., Precursor-derived covalent ceramics. *Adv. Mater.*, 1995, **7**, 775–787.
34. Bill, J., Schuhmacher, J., Müller, K., Schempp, S., Seitz, J., Dürr, J. *et al.*, Investigations on the structural evolution of amorphous Si–C–N ceramics from precursors. *Z. Metallkd.*, 2000, **91**, 335–351.
35. Riedel, R., Ruswisch, L. M., An, L. N. and Raj, R., Amorphous silicoboron carbonitride ceramic with very high viscosity at temperatures above 1500 °C. *J. Am. Ceram. Soc.*, 1998, **81**, 3341–3344.
36. Trimmel, G., Badheka, R., Babonneau, F., LaTournerie, J., Dempsy, P. and Bahloul-Houlier, D., Solid-state NMR and TG/MS study on the transformation of methyl groups during pyrolysis of preceramic precursors to SiCO glasses. *J. Sol–Gel Sci. Technol.*, 2003, **29**, 279–283.